Ab Initio Study of the Effect of Sulphur Concentration on the Structural, Electronic and Optical Properties of $CuIn(Se_1\text{-}_xS_x)_2$ Compound using Generalized Gradient Approximation

Moussa Merabet
Electronics Department, Faculty of Technology, University Ferhat Abbas of Setif 1, Algeria | Research Unit on Emerging Materials (RUEM), University Ferhat Abbas of Setif 1, Algeria
moussa.merabet.elect@gmail.com (corresponding author)

Idris Bouchama
Electronics Department, Faculty of Technology, University of Msila, Algeria | Research Unit on Emerging Materials (RUEM), University Ferhat Abbas of Setif 1, Algeria
bouchama.idris@yahoo.fr

Tayeb Chihi
Research Unit on Emerging Materials (RUEM), University Ferhat Abbas of Setif 1, Algeria
chihitayeb@ymail.com

Lamis Foudia
Research Unit on Emerging Materials (RUEM), University Ferhat Abbas of Setif 1, Algeria
foudialamis@gmail.com

Faycal Saidi
Electronics Department, Faculty of Technology, University of Ferhat Abbas Setif 1, Algeria | Research Unit on Emerging Materials (RUEM), University Ferhat Abbas of Setif 1, Algeria
faycal.adel1@gmail.com

Nadir Bouarissa
Laboratory of Material Physics and its Applications, University of Msila, Algeria
n_bouarissa@yahoo.fr

Received: 3 March 2025 | Revised: 7 April 2025 | Accepted: 24 April 2025

 DOI: https://doi.org/10.48084/etasr.10875

ABSTRACT

CuInSe2 (CIS) is a very promising material for thin film solar cells due to its unique optoelectronic properties. Sulfur (S) loading has been examined as an improvement to its performance. In this study, Density Functional Theory (DFT) calculations were used to evaluate the effect of S doping on the structural, electrical, and optical properties of CuIn $(Se_{1-x}S_x)_2$. The results show that S doping causes significant changes in the band structure and defect formation energy. The results obtained provide important insights into the potential of S-doped CIS as a high efficiency material for the fabrication of optoelectronic and photovoltaic devices.

Keywords-chalcopyrite; $CuIn(Se_{1-x}S_x)_2$; CASTEP; GGA-PBE approximation; thin-film solar cells; structural and electronic properties

I. INTRODUCTION

Solar cells used in the field of renewable energy, can convert solar to electrical energy. Chalcopyrite compounds, such as $CuInSe_2$, are widely utilized for manufacturing solar cells, due to their special properties [1], including high light absorption, ideal band gap [2], and thermal stability against photo-degradation [3]. The energy band gap is the property that distinguishes materials to conductors (very small or none band gap), insulators (large band gap), and semiconductors (small band gap). The band gap energy (E_g) is different for every semiconductor and affects the properties of the solar cells, with researchers trying to find ways to improve its efficiency [4-7]. One of the ways to improve the performance of CIS solar cells is sulfur doping, where part of the selenium is replaced by sulfur to form $CuIn(Se_{1-x}S_x)_2$. Authors in [8] prepared $CuIn(Se_{1-x}S_x)_2$ using a relatively simple and convenient solvothermal method, and studied the lattice constants and optical properties of the material. Authors in [9] fabricated $CuIn(Se_{1-x}S_x)_2$ crystals with the Bridgman technique using CuSe as a solvent, and examined the effect of sulfur on the electrical and optical properties of the material. Authors in [10] prepared $CuIn(Se_{1-x}S_x)_2$ thin films by precisely controlling the sulfurization temperature of CIS. Authors in [11] analyzed the effect of lattice volume on the bandgap of sulfur-doped CIS by first-principle calculations, while authors in [12] successfully deposited single phase $CuIn(Se_{1-x}S_x)_2$ using a two-step process. In addition, authors in [13] examined the optical properties of $CuIn(Se_{1-x}S_x)_2$ using spectroscopic ellipsometry. The purpose of this research is to investigate the structural, electrical, and optical properties of $CuIn(Se_{1-x}S_x)_2$ in the chalcopyrite phase for sulfur concentrations. First-principle calculations were performed based on DFT, as imported in the Cambridge Sequential Total Energy Package (CASTEP) program code [14, 15], in Materials Studio with the Generalized Gradient Approximation (GGA) [16]. The computational results were systematically compared with existing experimental and theoretical data. The main findings were summarized with a special focus on the potential applications of these materials in advanced optoelectronic devices.

II. COMPUTATIONAL DETAILS

Chalcopyrite compounds are efficient absorber materials widely used in high-performance thin-film photovoltaic devices [1, 17-19]. $CuIn(Se_{1-x}S_x)_2$ crystallizes as a chalcopyrite, with tetrahedral bonding. The unit cell of chalcopyrite is constituted by the stacking of two cubic zinc blende units along the c-axis. For CIS a 16-atom unit cell with the space group (I4) 2d is employed. The practice of sulfonation doping involves the substitution of sulfur atoms for selenium atoms in the chemical structure of a compound. The specific structure was analyzed using DFT [20] to obtain a more energetically stable form with optimum lattice volume and atomic locations. This study examined six concentrations of sulfur doping: x = 0, 0.2, 0.4, 0.6, 0.8, and 1. Employing first principle calculations based on DFT using the pseudo-potential method and the CASTEP software package in Material Studio, the study sought to analyze the effects of doping on the material's properties. The interaction between electrons and ions was modeled deploying the norm-conserving pseudo-potential method [21]. The calculations employed the GGA, represented by the Perdew-Burke-Ernzerhof (PBE) exchange-correlation functional [16], to analyze the structural and electronic properties of the system. These properties include, but are not limited to metrics, such as lattice constants, bulk modulus, first pressure derivatives, energy gap values, band structures, Total Density of States (TDOS), and Projected Density of States (PDOS) for both materials, as well as optical properties, involving optical dielectric function, refractive index, reflectivity, and absorption coefficient. The calculations were performed using a 9 × 9 × 5 Monkhorst-Pack [22] k-mesh and a plane wave energy cutoff of 900 eV. The electrical configuration of each element in $CuInX_2$ (X=S, Se) is: Cu: $3d^{10}$ $4s^1$, Se (S): $3s^2$ $3p^4$ and In: $4d^{10}$ $5s^2$ $5p^1$.

III. RESULTS AND DISCUSSION

A. Structural Properties

$CuInSe_2$ crystallizes in the chalcopyrite structure, as shown in Figure 1. This phenomenon persists even following the introduction of sulfur through doping, resulting in the same crystalline structure where the sulfur (S) atom can substitute the selenium (Se) atom.

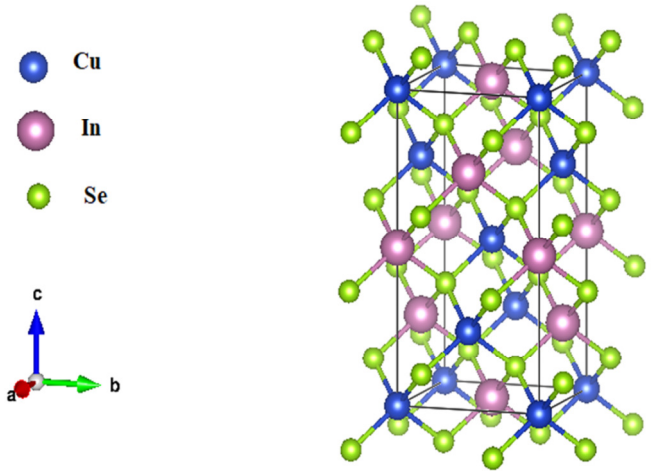

Fig. 1. Graphical presentation in 3D of chalcopyrite $CuInSe_2$.

The structural characteristics, including equilibrium lattice constants (a) and (c), bulk modulus (B), and the first pressure derivative (B'), were studied by fitting Murnaghan's equation of state [23] to the total energy as a function of the volume curves obtained from the GGA-PBE approximation. The structures of $CuIn(Se_{1-x}S_x)_2$ were optimized at varying pressures, as presented in Figure 2. The relationship between total energy and volume was described by:

$$E(V) = E_0 + \left[\frac{B_0 V}{B'(B'-1)}\right].\left[B'\left(1-\frac{V_0}{V}\right) + \left(\frac{V_0}{V}\right)^{B'} - 1\right] \quad (1)$$

where V_0, B_0, and $B_0{}'$ represent the equilibrium volume, the bulk modulus, and its derivative, respectively. The compressibility modulus and its pressure derivative B' are expressed as:

$$B_0' = \frac{\partial B}{\partial p} \quad (2)$$

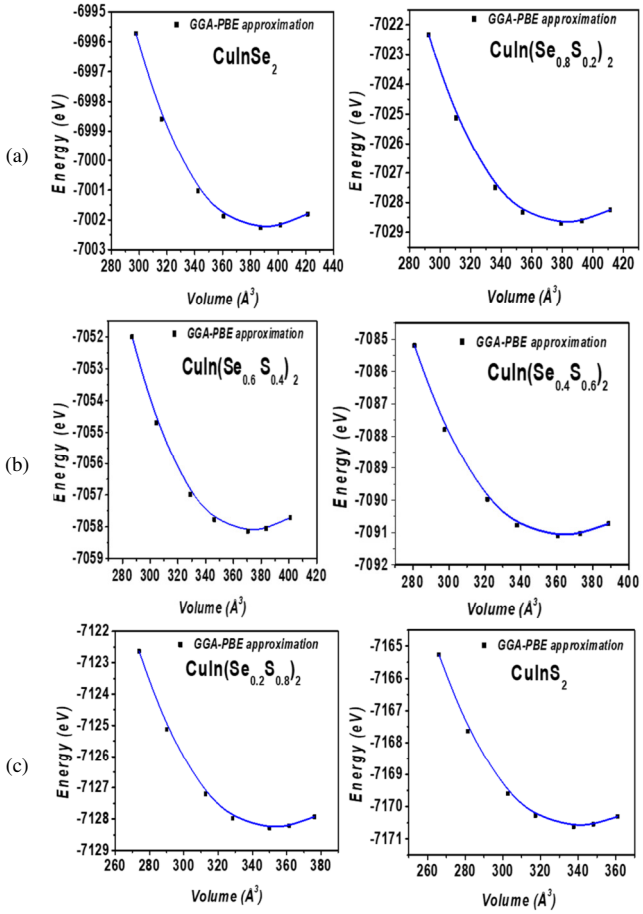

Fig. 2. Calculated total energy as a function of unit cell volume for chalcopyrite $CuIn(Se_{1-x}S_x)_2$: (a) x=0 (left), x=0.2 (right), (b) x=0.4 (left), x=0.6 (right), (c) x=0.8 (left), x=1 (right).

Table I presents the results of the improved structural parameters for $CuIn(Se_{1-x}S_x)_2$ compounds. Conversely, an increase in sulfur (S) levels has been observed to result in a concomitant decrease in both *a* and *c*. This outcome is reasonable given that the effective ionic radii of S_2- (17 Å) are less than those of Se_2- (18.4 Å) [24]. The calculated lattice parameters demonstrate a strong correlation with both the experimental and theoretical data for $CuIn(Se_{1-x}S_x)_2$.

B. Electronic Properties

The examination of the band structure is important for the analysis of the physical characteristics of materials. The method enables the estimation of several key properties, including the absorption spectral distribution, the charge density distribution, the electron and hole mobility, and other related properties. This section presents the energy band structure along multiple symmetry directions that have been estimated, as well as the density of states in the $CuIn(Se_{1-x}S_x)_2$ compounds. As shown in Figure 3, these compounds exhibit a direct band gap, noting that the experimental band gap values for these compounds differ from the present study's current calculations. This deviation can be attributed to the adoption of the GGA within DFT to handle the exchange-correlation potential. The band structure of $CuIn(Se_{1-x}S_x)_2$ has been computed, and the results are displayed for six different S concentration values (x = 0, 0.2, 0.4, 0.6, 0.8, 1). All Fermi levels (dashed lines) have been set to zero. The energy gap increases in proportion to the S content, a finding that aligns with experimental results.

TABLE I. CRYSTAL STRUCTURE PARAMETERS OF $CUIN(SE_{1-X}S_X)_2$ COMPOUNDS

Compound	*a* (Å)	*c* (Å)	*c/a*	B_0(GPa)	B_0
$CuInSe_2$ (Present work)	5.802	11.504	1.982	58.752	4.40
Expt. [25]	5.780	11.55	1.998		
Theo. [26]	5.8455	11.683	1.998		
Theo. [27]	5.592	11.285	2.018	68.7	3.57
Theo. [28]	5.817	11.743	2.018	54.56	4.89
Theo. [29]	5.883	11.842	2.013	54.200	
Expt. [30]	5.517	11.122	2.015		
Expt. [31]	5.814	11.63	2.0003		
Expt. [32]	5.561 ±0.002	11.116 ±0.007		75 ± 5	4.00
Theo. [25]	5.862	11.792	2.012		
$CuIn(Se_{0.8}S_{0.2})_2$	5.761	11.427	1.983	62.497	4.36
$CuIn(Se_{0.6}S_{0.4})_2$	5.717	11.334	1.982	64.257	4.361
$CuIn(Se_{0.4}S_{0.6})_2$	5.664	11.237	1.983	66.788	4.21
$CuIn(Se_{0.2}S_{0.8})_2$	5.607	11.130	1.983	69.233	4.21
$CuInS_2$ (Present work)	5.538	11.007	1.987	70.769	4.32
Expt. [25]	5.520	11.080	2.007		
Expt. [28]	5.574	11.248	2.017	65.81	4.80
Theo. [25]	5.576	11.251	2.018		
Theo. [26]	5.5734	11.228	2.02		
Theo. [29]	5.598	11.277	2.014	65.547	

The valence band of all compounds is divided into three sub-bands, as presented in the total DOS diagram in Figure 4. The uppermost valence sub bands are found between the Fermi level and approximately 2 eV below it. These sub bands are primarily contributed by the hybridization of the Cu-*d* states and Se-*p* states at $CuInSe_2$; however, for $CuInS_2$, the hybridization occurs between the Cu-*d* states and S-*p* states.

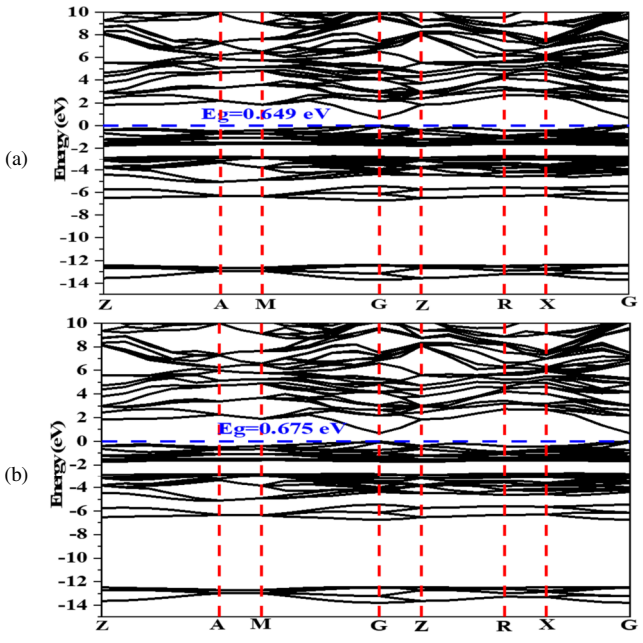

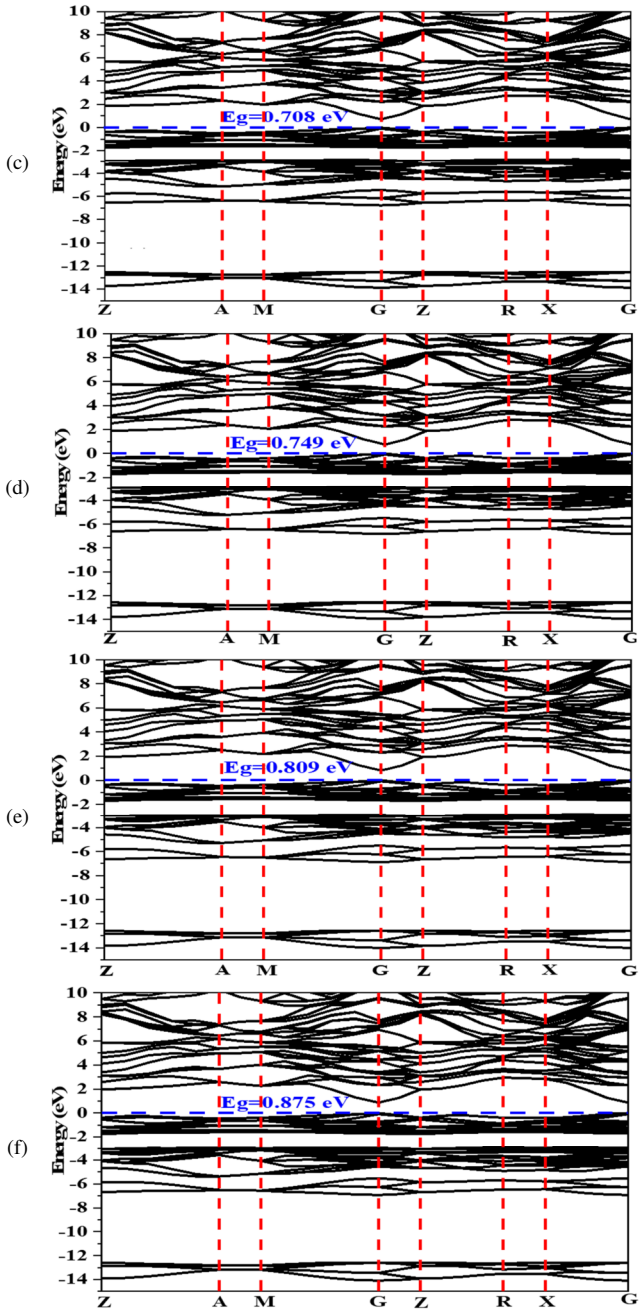

Fig. 3. Band structure curves for chalcopyrite CuIn $(Se_{1-x}S_x)_2$:(a) x =0, (b) x =0.2, (c) x =0.4, (d) x =0.6, (e) x =0.8, (f) x =1, with GGA approximation.

The lowest sub-band is situated between -12 eV and -4 eV and originates primarily from Se-s states, with minor contributions from In-s and In-p states. The middle sub-band ranges from approximately -3 eV to -7 eV, with states representing a hybridization of Se-*p* and In-*s* (and In-*p*) states. The Fermi level is set at 0 eV, and is controlled by the Cu-*d* and Se-*p* states (valence band) and the In-*s* states (conduction band). As shown in Figure 4, the conduction bands are primarily composed of states originating from the Cu-*p*, Se-*p*, In-*s*, and In-*p* orbitals. For $CuInSe_2$, there is no distinction between its DOS and that of $CuInS_2$; the principal disparities emerging as the states of Se-*p* and Se-*s* are progressively supplanted by the states of S-*p* and S-*s* with the rise in x in $CuIn(Se_{1-x}S_x)_2$. The position of the Conduction Band Minimum (CBM) exhibits an upward shift as S atoms are substituted with Se atoms. This phenomenon can be attributed to the increase in energy level from Se to S. This shift is likely the primary cause of the increasing energy gap in $CuIn(Se_{1-x}S_x)2$.

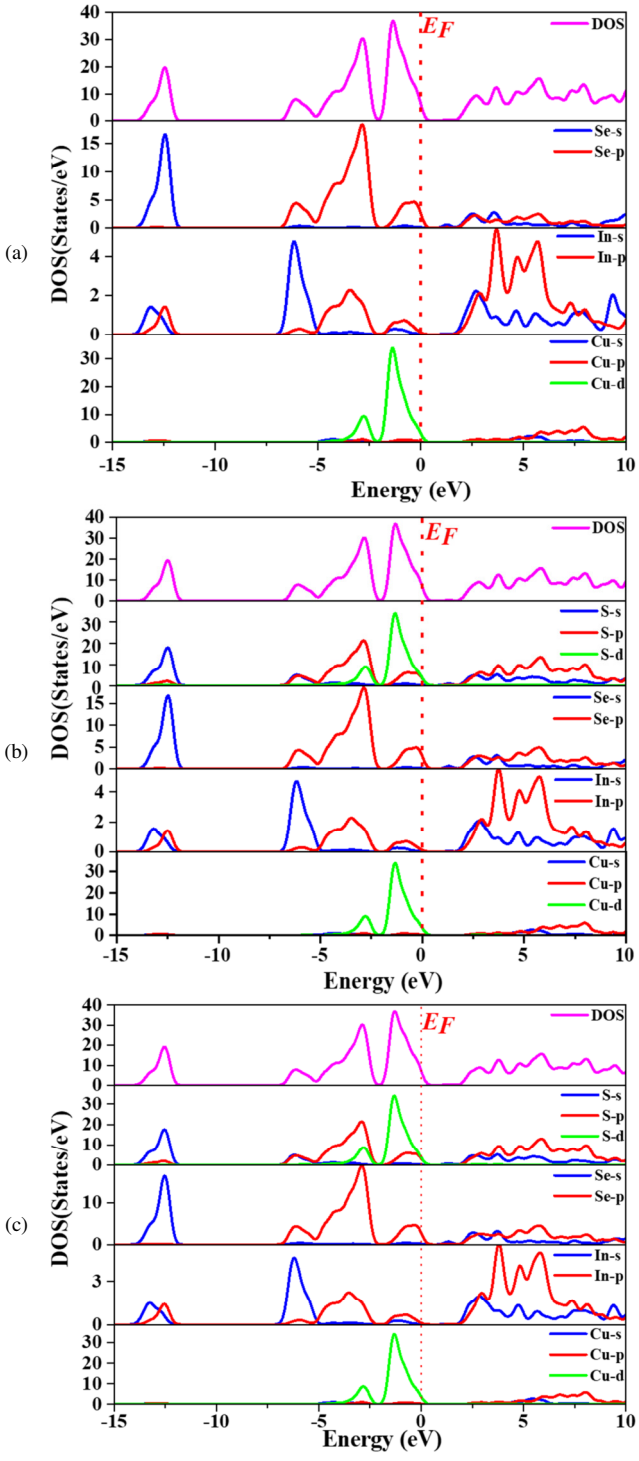

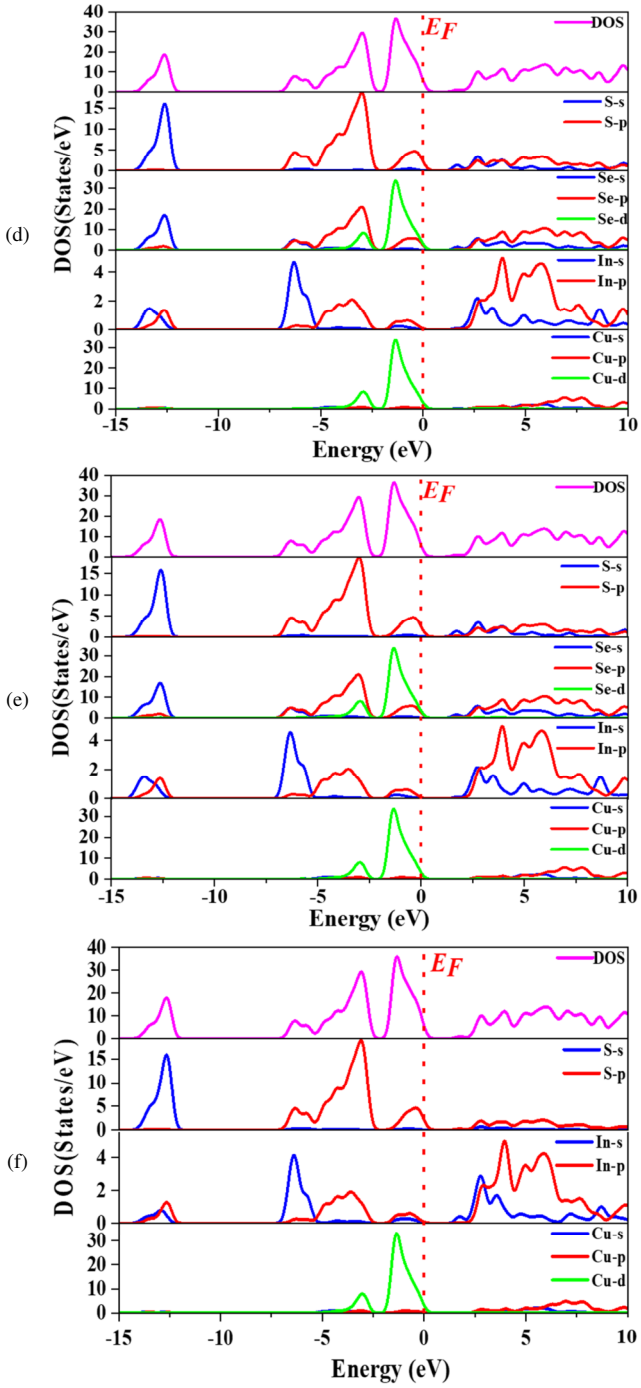

Fig. 4. DOS and PDOS for chalcopyrite CuIn $(Se_{1-x}S_x)_2$: (a) x =0, (b) x =0.2, (c) x =0.4, (d) x =0.6, (e) x =0.8, (f) x =1, with GGA approximation.

The energy band gap undergoes a non-linear change in accordance with the rise in sulfur concentration, as presented by the following equation:

$$Eg(x) = 0.650 + 0.096x + 0.129x^2 \quad (3)$$

Table II presents the calculated band gap (Eg) within GGA approximations of chalcopyrite $CuIn(Se_{1-x}S_x)_2$ compound.

TABLE II. CALCULATED BAND GAP WITHIN GGA APPROXIMATIONS OF CHALCOPYRIT $CuIn(Se_{1-x}S_X)_2$ COMPOUND, COMPARED WITH EXPERIMENTAL AND OTHER THEORETICAL WORKS

Materials	*Eg*	*Eg*	*Eg*
	Present work	Expt.	Theo.
$CuInSe_2$	0.649	0.98 [33] 1 [34]	1.07 [24] 0.8 [34]
$CuIn(Se_{0.8}S_{0.2})_2$	0.676		
$CuIn(Se_{0.6}S_{0.4})_2$	0.709		
$CuIn(Se_{0.4}S_{0.6})_2$	0.752		
$CuIn(Se_{0.2}S_{0.8})_2$	0.811		
$CuInS_2$	0.875	1.43 [30]	1.384 [24] 0.821 [34]

C. Optical Properties

The analysis of a material's optical spectrum is a powerful tool for understanding the behavior of solids. In this study the material properties are examined through various techniques, such as absorption, reflection, and light emission. However, ternary chalcopyrite semiconductors possess distinctive optical properties, thereby facilitating research in a variety of disciplines. Consequently, the development of accurate methods grounded in first principles is important in order to ensure a precise description of these properties. The GGA approximation was used to calculate the optical characteristics of the compound $CuIn(Se_{1-x}S_x)_2$. Two values of x were considered: x = 0 and x = 1. The dielectric function, optical conductivity, refractive index, reflectivity, and absorption coefficient were included in the calculations, which were performed to determine the optimal bandgap values. The optical dielectric constant, static reflectivity, and static refractive index for the chalcopyrite CuIn $(Se_{1-x}S_x)_2$ compound were measured and compared with experimental and other theoretical works [35, 36].

1) Dielectric Function

The dielectric functions of CuIn $(Se_{1-x}S_x)_2$ (x=0,1), which are materials used in thin-film solar cells, are significant for understanding their optical and electrical properties. The dielectric function is defined as the property of matter that governs its interaction with electromagnetic radiations, including light. The dielectric function of these materials is typically described by two main components: the real part (ε_1) and the imaginary part (ε_2). The complex dielectric function $\varepsilon(\omega)$ of semiconductor materials is:

$$\varepsilon(\omega) = \varepsilon_{real}(\omega) + i\varepsilon_{imaginary}(\omega) \quad (4)$$

and can be used to calculate other optical parameters, such as the absorption coefficient $\alpha(\omega)$, the refractive index $n(\omega)$, and the reflectivity $R(\omega)$. The imaginary part of the dielectric function is:

$$\varepsilon_{\alpha\beta}^{(2)}(\omega) = \frac{4\pi^2 e^2}{\Omega} \lim_{q\to 0} \frac{1}{q^2} \sum_{c,v,k} 2\boldsymbol{w_k}\boldsymbol{\delta}(\varepsilon_{ck} - \varepsilon_{vk} - \omega) \times \langle \boldsymbol{u_{ck}} + \boldsymbol{e_{\alpha q}} | \boldsymbol{u_{vk}} \rangle \langle \boldsymbol{u_{ck}} + \boldsymbol{e_{\beta q}} | \boldsymbol{u_{vk}} \rangle \quad (5)$$

where $\boldsymbol{u_{ck}}$ is the cell periodic component of the wave function at the k-point, $\boldsymbol{e_\alpha}$ and $\boldsymbol{e_\beta}$ are unit vectors for the three Cartesian directions, and $\boldsymbol{c}$ and $\boldsymbol{v}$ are the indices of the conduction and valence band states, respectively. The Kramers–Kronig bidirectional mathematical relation connects the imaginary and real parts of any complex function that is analytic in the upper

half-plane. The real part of the dielectric function can be obtained from the imaginary part using [37, 38]:

$$\varepsilon_{\alpha\beta}^{(1)}(\omega) = 1 + \frac{2}{\pi} P \int_0^{\infty} \frac{\varepsilon_{\alpha\beta}^{(2)}(\omega\prime)\omega\prime}{\omega\prime^2 - \omega^2 + i\eta} \, d\omega' \quad (6)$$

where the principal value is represented by P. In the Kramers–Kronig transformation [39] a small complex shift η is used, which in this work's calculations is set at 0.1 eV. The knowledge of both the real and imaginary parts of the dielectric function can help in calculating other optical properties. An examination of the optical properties was made under two types of polarizations: ordinary along the x and y directions ($E//$ (100)) and extraordinary along the z direction ($E//$ (001)). As shown in Figure 5, the plots of the real part of the dielectric function are presented as a function of photon energy for $CuIn(Se_{1-x}S_x)_2$ (x = 0, 1), covering a range of 0 eV to 20 eV. The zero-frequency limit $\varepsilon_1(0)$, is a critical quantity governed by the band gap of the material. The calculated values of $\varepsilon_1(0)$ employing the GGA-PBE approximation are presented in Table III, exhibiting strong concurrence with the theoretical and experimental outcomes derived under ordinary and extraordinary polarization for both chalcopyrite compounds. The imaginary part of the dielectric function, $\varepsilon_2(\omega)$, is indicative of the optical response of a material and provides essential information regarding the inter-band electronic transitions occurring between the valence and conduction bands. These transitions occur when photons with sufficient energy excite electrons from occupied states in the valence band to unoccupied states in the conduction band, influencing the material's optical absorption properties, and the results align with the theoretical curves and the experimental data [40–42].

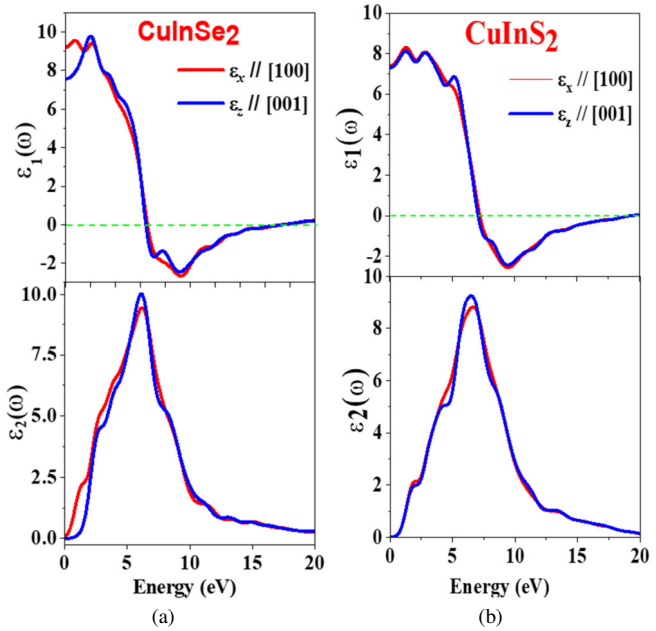

Fig. 5. Real and imaginary part of dielectric function for chalcopyrite: (a) $CuInSe_2$ and (b) $CuInS_2$ compound.

For $CuInSe_2$(x=0) the peak of $\varepsilon_1(\omega)$ is close to 6 eV, indicating strong refractive properties in this energy spectrum. It also means that light interacts with the structure more effectively since it is much concentrated within the material at this intensity.

TABLE III. CALCULATED $\varepsilon_1(0)$, $R(0)$, AND $n(0)$ WITHIN GGA OF CHALCOPYRITE $CuIn(Se_{1-x}S_x)_2$ COMPARED WITH EXPERIMENTAL AND OTHER THEORETICAL WORKS

Static parameters	$\varepsilon_1(0)$		$R(0)$		$n(0)$	
Materials	E//(100)	E//(001)	E//(100)	E//(001)	E//(100)	E//(001)
$CuInSe_2$ (x=0)	9.314	7.577	0.252	0.218	3.06	2.753
[35]	8.95	8.44	0.25	0.24	2.99	2.90
[36]					2.937	2.950
$CuInS_2$ (x=1)	7.422	7.340	0.227	0.213	2.728	2.709
[26]	7.63				2.76	

At higher energies (above ~10 eV), the plasma frequency, is defined as the point at which the material transitions from being more reflective to more absorptive. The significant peak of $\varepsilon_2(\omega)$ around 4 eV signifies robust absorption resulting from inter-band electronic transitions. This phenomenon is indicative of the material's capacity to absorb incident photons and generate electron-hole pairs, a process that is essential for photovoltaic applications. For $CuInS_2$ (x=1), the real part ($\varepsilon_1(\omega)$) exhibits a peak at slightly lower energy (~5.5 eV), indicative of strong refractive behavior within this range. The real part crosses the zero line at higher energies (8 eV – 10 eV) at the plasma frequency. The imaginary part ($\varepsilon_2(\omega)$) displays an attractive absorption peak at 3.5 eV, which is slightly lower than that of $CuInSe_2$. This finding indicates that $CuInS_2$ is well-suited for absorbing lower-energy photons, thereby making it a suitable complement to $CuInSe_2$ in solar energy harvesting applications. This enhancement is poised to enhance the efficiency of solar cells. The dielectric functions of $CuInSe_2$ and $CuInS_2$ are indicative of their optical characteristics and demonstrate their great potential for application in solar cell technology. While $CuInS_2$ demonstrates efficacy in the short-wave length region, $CuInSe_2$ exhibits superiority in long-wave length light absorption. The combination of Se and S in $CuIn(Se_{x-1}S_x)_2$ results in the formation of effective tandem solar cells, thereby maximizing the usage of the solar spectrum and enhancing energy conversion efficiency.

2) Reflectivity

The reflectivity R can be calculated from the refractive indices n and k [43], which is applicable only when an incident wave in a vacuum strikes a dielectric material at normal incidence:

$$R = \frac{(n-1)^2 + k^2}{(n+1)^2 + k^2} \quad (7)$$

The reflective index is expressed as the ratio of the speed of light in a vacuum relative to that of the medium under consideration. The calculated values of R (0) using the GGA-PBE approximation show strong agreement with both the theoretical and experimental results obtained under ordinary and extraordinary polarization for the two chalcopyrite compounds. As presented in Figure 6, the reflectivity spectra for the samples under consideration span the photon energy range from 0 to 20 eV. $CuInSe_2$ (x=0) displays enhanced and more pronounced reflectivity within the energy range of 1 eV - 4 eV, suggesting an augmented interaction with incident light.

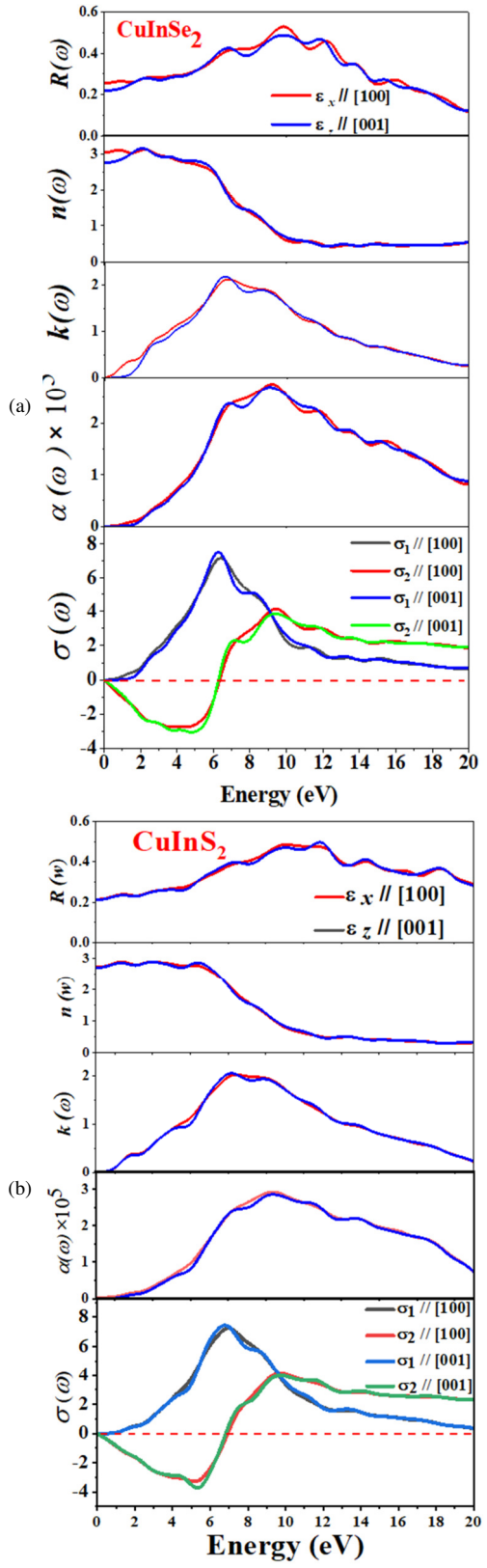

Fig. 6. Optical properties ($R(\omega)$: reflectivity, $n(\omega)$: refractive index, $k(\omega)$: extinctive index, $\alpha(\omega)$: absorption coefficient, $\sigma(\omega)$: optical conductivity of CuIn $(Se_{1-x}\ S_x)_2$ at: (a) x=0, (b) x=1.

This increased reflectivity in the low-energy region, attributable to a diminished band gap, permits enhanced light reflection. However, as the S-doping level increases and the material transitions to $CuInS_2$ (x=1), the reflectivity in the low-energy region experiences a slight decline. The larger band gap restricts the interaction with lower-energy photons, thus enhancing the material's transparency within this region. An enhancement in the high-energy region (>6 eV) has been observed, where the reflectivity of $CuInS_2$ becomes more uniform and comparable to that of $CuInSe_2$. This shift in reflectivity serves to offset the observed variations.

3) Refractive and Extinctive Indexes

The complex refractive index N has real and imaginary factors, which are the extinction coefficient k and the refractive index n, respectively [24, 44], when $N = \sqrt{\varepsilon(\omega)} = n + ik$ so, n and k can be determined as:

$$n = \left(\frac{\sqrt{\varepsilon_1^2(\omega)+\varepsilon_2^2(\omega)}+\varepsilon_1}{2} \right)^{1/2} \quad (8)$$

$$k = \left(\frac{\sqrt{\varepsilon_1^2(\omega)+\varepsilon_2^2(\omega)}-\varepsilon_1}{2} \right)^{1/2} \quad (9)$$

It was observed that both $CuInSe_2$ and $CuInS_2$ converge at higher energies; however, $CuInSe_2$ exhibits a higher refractive index at lower energies (<3 eV). This finding suggests that $CuInSe_2$ has a stronger interaction with low-energy photons and more light bending. Conversely, $CuInS_2$ exhibits a lower refractive index within this spectral range. The extinction coefficient $k(\omega)$ of $CuInSe_2$ is greater, reaching its maximum at lower energies (~2 eV - 6 eV) and showing stronger light absorption with a gradual decrease at higher energies. In contrast, the $k(\omega)$ values of $CuInS_2$ are lower across the spectrum, indicating less absorption losses. S-doping in $CuIn(Se_{x-1}S_x)_2$ enhances optical properties by decreasing the refractive index n, increasing light transmission at lower energies, and adjusting the extinction coefficient k, thereby enhancing transparency in the visible range while increasing absorption at higher energies. These properties render them particularly well-suited for photovoltaic applications.

4) Absorption Coefficient

The absorption coefficient $\alpha(\omega)$ determines how far the light of a specific wavelength may enter a material before being absorbed. It can be calculated directly from the dielectric function using [24,44]:

$$\alpha(\omega) = \sqrt{2}\omega \left[\sqrt{\varepsilon_1^2(\omega) + \varepsilon_2^2(\omega)} - \varepsilon_1(\omega) \right]^{1/2} = 2\omega \quad (10)$$

Figure 6 depicts the absorption spectra of CuIn $(Se_{1-x}S_x)_2$, with different doping densities (x = 0, 1). Absorption spectra provide an approximation of the optical band gap. Absorption occurs when the energy of a photon exceeds the band gap, causing electrons in the valence band to become energized and move to the conduction band. In instances where the photon energy is less than the band gap, the material exhibits a lack of absorption, hence enabling the transmission of light through the

material, a property that can be defined as transparent to light. When the photon energy exceeds the band gap, the absorption rate experiences a substantial increase, therefore shaping the absorption edge. As the *x*-axis increases, the absorption edge shifts toward higher photon energy ($h\nu$), suggesting an increase in the band gap (Eg). This phenomenon signifies the material's augmented capacity to absorb high-energy photons. Distinct absorption peaks are observed at 8 eV and 11 eV, with intensity and location variations attributable to changes in electronic structure and optical transitions. The material is transparent below the bandgap ($h\nu$ <Eg), which expands with increasing *x* due to the widening bandgap. The absorption spectra undergo a substantial change above 6 eV, which is most likely attributable to higher-order transitions driven by S-doping.

5) Optical Conductivity

As presented in Figure 6, the electronic response to light is more significant in the lower energy range (~3 eV - 6 eV), where the peaks of $CuInSe_2$ are observed. In contrast, $CuInS_2$ exhibits peaks at slightly higher energies (~4 eV – 7 eV), though with lower maximum values in comparison to $CuInSe_2$. Consequently, $CuInSe_2$ exhibits stronger optical conductivity, $\sigma(\omega)$, at lower photon energies, rendering it more responsive to low-energy light. Conversely, $CuInS_2$ demonstrates superior performance at slightly higher photon energies. In the present study, the effective mass of electrons and holes subsequent to sulfur incorporation was not calculated. Nonetheless, this has been achieved for $InAs_xSb_{1-x}$, as evidenced by the observation of a deviation from linearity resulting from the bowing effect. The non-linearity of the effective mass of heavy-holes is an inherent property of the system under study [45].

IV. CONCLUSIONS

Density Functional Theory (DFT) calculations have been performed to study the structural, electrical, and optical properties of $CuInSe_2$ chalcopyrite materials doped with sulfur (*S*) as *x* increased from 0 to 1, using the Generalized Gradient Approximation - Perdew-Burke-Ernzerhof (GGA-PBE) approximation. The results of this study include data on the complex dielectric function, refractive index, extinction coefficient, reflectivity, bandgap, and absorption coefficient of $CuIn(Se_{1-x}S_x)_2$. The observed energy gap values are reasonably similar to the experimental results and significantly better than previously reported theoretical values. Furthermore, it was observed that certain theoretical values, including B0 and B0', as well as the calculation of their band gap, have been cited for the first time in the context of $CuIn(Se_{1-x}S_x)_2$ compounds doped with sulfur. S-doping of $CuIn(Se_{x-1}\ S_x)_2$ improves optical properties by lowering the refractive index, improving low-energy light transmission, and adjusting the extinction coefficient. This doping enhances transparency in the visible range while increasing absorption at high energy levels. Consequently, it is well-suited for photovoltaic applications. $CuInSe_2$ demonstrates higher optical conductivity at low photon energies, rendering it more responsive to low-energy light, while $CuInS_2$ exhibits superior performance at slightly higher photon energies. The $CuIn(Se_{1-x}S_x)_2$ materials demonstrate considerable potential for usage in solar cell applications and advanced optoelectronic devices. The practical integration of $CuIn(Se_{1-x}S_x)_2$ poses several technical challenges, including thermal stability, fabrication complexity, and production costs.

REFERENCES

[1] W.-J. Wang *et al.*, "Synthesis of CuInSe2 monodisperse nanoparticles and the nanorings shape evolution via a green solution reaction route," *Materials Science in Semiconductor Processing*, vol. 15, no. 5, pp. 467–471, Oct. 2012, https://doi.org/10.1016/j.mssp.2012.03.001.

[2] S. Cui, W. Feng, H. Hu, Z. Feng, and Y. Wang, "Structural and electronic properties of ZnO under high pressure," *Journal of Alloys and Compounds*, vol. 476, no. 1, pp. 306–310, May 2009, https://doi.org/10.1016/j.jallcom.2008.08.052.

[3] A. M. Fernández and R. N. Bhattacharya, "Electrodeposition of CuIn1−xGaxSe2 precursor films: optimization of film composition and morphology," *Thin Solid Films*, vol. 474, no. 1, pp. 10–13, Mar. 2005, https://doi.org/10.1016/j.tsf.2004.02.104.

[4] D. A. Tuan, P. Vu, and N. V. Lien, "Design and Control of a Three-Phase T-Type Inverter using Reverse-Blocking IGBTs," *Engineering, Technology & Applied Science Research*, vol. 11, no. 1, pp. 6614–6619, Feb. 2021, https://doi.org/10.48084/etasr.3954.

[5] A. S. Al-Ezzi, M. N. M. Ansari, and N. Tan, "Flexible and freestanding solar cells based on metal organic chemical vapour deposition- grown graphene," *Chemical Papers*, vol. 79, no. 4, pp. 2019–2036, Apr. 2025, https://doi.org/10.1007/s11696-025-03910-2.

[6] A. S. I. Al-Ezzi and M. N. M. Ansari, "Analytical modelling and performance study of single-junction GaAs-based solar cell efficiency," *Journal of the Korean Physical Society*, vol. 86, no. 3, pp. 245–262, Feb. 2025, https://doi.org/10.1007/s40042-024-01260-y.

[7] A. S. Al-Ezzi and M. N. M. Ansari, "Numerical analysis and performance study of a double-heterojunction GaAs-based solar cell," *Journal of Computational Electronics*, vol. 23, no. 2, pp. 358–368, Apr. 2024, https://doi.org/10.1007/s10825-023-02126-5.

[8] J. Xiao, Y. Xie, Y. Xiong, R. Tang, and Y. Qian, "A mild solvothermal route to chalcopyrite quaternary semiconductor CuIn(SexS1 − x)2 nanocrystallites," *Journal of Materials Chemistry*, vol. 11, no. 5, pp. 1417–1420, Jan. 2001, https://doi.org/10.1039/B100092F.

[9] S. Bandyopadhyaya, S. Roy, S. Chaudhuri, and A. K. Pal, "CuIn(SxSe1−x)2 films prepared by graphite box annealing of In/Cu stacked elemental layers," *Vacuum*, vol. 62, no. 1, pp. 61–73, May 2001, https://doi.org/10.1016/S0042-207X(01)00156-7.

[10] G. Wang *et al.*, "Preparation of CuIn(SxSe1-x)2 thin films with tunable band gap by controlling sulfurization temperature of CuInSe2," *Journal of Materials Research*, vol. 25, no. 12, pp. 2426–2429, Dec. 2010, https://doi.org/10.1557/jmr.2010.0304.

[11] C. Xiang, Z. Yujun, Y. Ruohe, and H. Julong, "Impact of lattice volume on the band gap broadening of isovalent S-doped CuInSe2," *Journal of Semiconductors*, vol. 29, no. 10, pp. 1883–1888, 2008.

[12] C. J. Sheppard, V. Alberts, and J. R. Botha, "Structural and optical characterization of single-phase CuIn(Se,S)2 thin films deposited using a two-step process," *Physica Status Solidi C*, vol. 5, no. 2, pp. 641–644, 2008, https://doi.org/10.1002/pssc.200776837.

[13] K. Zeaiter and C. Llinarès, "Optical properties of the quaternary alloy system CuIn(SxSe1−x)2 investigated by spectroscopic ellipsometry," *Journal of Applied Physics*, vol. 86, no. 12, pp. 6822–6825, Dec. 1999, https://doi.org/10.1063/1.371757.

[14] M. D. Segall *et al.*, "First-principles simulation: ideas, illustrations and the CASTEP code," *Journal of Physics: Condensed Matter*, vol. 14, no. 11, Mar. 2002, Art. no. 2717, https://doi.org/10.1088/0953-8984/14/11/301.

[15] S. J. Clark *et al.*, "First principles methods using CASTEP," *Zeitschrift für Kristallographie - Crystalline Materials*, vol. 220, no. 5–6, pp. 567–570, May 2005, https://doi.org/10.1524/zkri.220.5.567.65075.

[16] J. P. Perdew, K. Burke, and M. Ernzerhof, "Generalized Gradient Approximation Made Simple," *Physical Review Letters*, vol. 77, no. 18, pp. 3865–3868, Oct. 1996, https://doi.org/10.1103/PhysRevLett. 77.3865.

[17] E. Kask, M. Grossberg, R. Josepson, P. Salu, K. Timmo, and J. Krustok, "Defect studies in Cu2ZnSnSe4 and Cu2ZnSn(Se0.75S0.25)4 by admittance and photoluminescence spectroscopy," *Materials Science in Semiconductor Processing*, vol. 16, no. 3, pp. 992–996, Jun. 2013, https://doi.org/10.1016/j.mssp.2013.02.009.

[18] M. A. Contreras, H. Wiesner, J. Tuttle, K. Ramanathan, and R. Noufi, "Issues on the chalcopyrite/defect-chalcopyrite junction model for high-efficiency Cu(In,Ga)Se2 solar cells " *Solar Energy Materials and Solar Cells*, vol. 49, no. 1, pp. 239–247, Dec. 1997, https://doi.org/10.1016/S0927-0248(97)00200-6.

[19] R. Herberholz, V. Nadenau, U. Rühle, C. Köble, H. W. Schock, and B. Dimmler, "Prospects of wide-gap chalcopyrites for thin film photovoltaic modules," *Solar Energy Materials and Solar Cells*, vol. 49, no. 1, pp. 227–237, Dec. 1997, https://doi.org/10.1016/S0927-0248(97)00199-2.

[20] J. Pohl and K. Albe, "Thermodynamics and kinetics of the copper vacancy in CuInSe2, CuGaSe2, CuInS2, and CuGaS2 from screened-exchange hybrid density functional theory," *Journal of Applied Physics*, vol. 108, no. 2, Jul. 2010, Art. no. 023509, https://doi.org/10.1063/1.3456161.

[21] D. Vanderbilt, "Soft self-consistent pseudopotentials in a generalized eigenvalue formalism," *Physical Review B*, vol. 41, no. 11, pp. 7892–7895, Apr. 1990, https://doi.org/10.1103/PhysRevB.41.7892.

[22] H. J. Monkhorst and J. D. Pack, "Special points for Brillouin-zone integrations," *Physical Review B*, vol. 13, no. 12, pp. 5188–5192, Jun. 1976, https://doi.org/10.1103/PhysRevB.13.5188.

[23] F. D. Murnaghan, "The Compressibility of Media under Extreme Pressures," *Proceedings of the National Academy of Sciences*, vol. 30, no. 9, pp. 244–247, Sep. 1944, https://doi.org/10.1073/pnas.30.9.244.

[24] F. C. Wan *et al.*, "First-principles investigation of the optical properties of CuIn(SxSe1–x)2," *Materials Science in Semiconductor Processing*, vol. 16, no. 6, pp. 1422–1427, Dec. 2013, https://doi.org/10.1016/j.mssp.2013.05.009.

[25] V. L. Shaposhnikov, A. V. Krivosheeva, V. E. Borisenko, J.-L. Lazzari, and F. A. d'Avitaya, "Ab initio modeling of the structural, electronic, and optical properties of $A^{II}B^{IV}C_2^{V}$ semiconductors," *Physical Review B*, vol. 85, no. 20, May 2012, Art. no. 205201, https://doi.org/10.1103/PhysRevB.85.205201.

[26] P. Nayebi, K. Mirabbaszadeh, and M. Shamshirsaz, "Density functional theory of structural, electronic and optical properties of CuXY2 (X=In, Ga and Y=S, Se) chalcopyrite semiconductors," *Physica B: Condensed Matter*, vol. 416, pp. 55–63, May 2013, https://doi.org/10.1016/j.physb.2013.02.015.

[27] B. I. Adetunji, "Pressure effect on the structural and electronic properties of CuInS2," *Solid State Sciences*, vol. 55, pp. 42–47, May 2016, https://doi.org/10.1016/j.solidstatesciences.2016.02.004.

[28] E. Mazalan, M. S. A. Aziz, N. A. S. Amin, F. D. Ismail, M. S. Roslan, and K. Chaudhary, "First-principles study on crystal structures and bulk modulus of CuInX2 (X = S, Se, S-Se) solar cell absorber," *Journal of Physics: Conference Series*, vol. 2432, no. 1, Feb. 2023, Art. no. 012009, https://doi.org/10.1088/1742-6596/2432/1/012009.

[29] J.-W. Yang and L. An, "First-principles determination of pressure-induced structure, anisotropic elasticity and ideal strengths of CuInS2 and CuInSe2," *Solid State Communications*, vol. 316–317, Aug. 2020, Art. no. 113952, https://doi.org/10.1016/j.ssc.2020.113952.

[30] H. L. Hwang, C. Y. Sun, C. Y. Leu, C. L. Cheng, and C. C. Tu, "Growth of CuInS2 and its characterization," *Revue de Physique Appliquée*, vol. 13, no. 12, 1978, Art. no. 745, https://doi.org/10.1051/rphysap:019780013012074500.

[31] M. L. Fearheiley, K. J. Bachmann, Y.-H. Shing, S. A. Vasquez, and C. R. Herrington, "The lattice constants of CuInSe2," *Journal of Electronic Materials*, vol. 14, no. 6, pp. 677–683, Nov. 1985, https://doi.org/10.1007/BF02654305.

[32] T. Tinoco, A. Polian, D. Gomez, and J. P. Itie, "Structural Studies of CuInS2 and CuInSe2 under High Pressure," *Physica Status Solidi (b)*, vol. 198, no. 1, pp. 433–438, 1996, https://doi.org/10.1002/pssb.2221980156.

[33] M. Belhadj, A. Tadjer, B. Abbar, Z. Bousahla, B. Bouhafs, and H. Aourag, "Structural, electronic and optical calculations of Cu(In,Ga)Se2 ternary chalcopyrites," *physica status solidi (b)*, vol. 241, no. 11, pp. 2516–2528, 2004, https://doi.org/10.1002/pssb.200302045.

[34] A. Sajid, S. Sibghat-Ullah, G. Murtaza, R. Khenata, A. Manzar, and S. B. Omran, "Electronic structure and optical properties of chalcopyrite CuYZ2 (Y=Al, Ga, In; Z=S, Se): an ab initio study," *Journal of Optoelectronics and Advanced Materials*, vol. 16, no. 1–2, pp. 76–81, 2014.

[35] M. Hadjab, M. Ibrir, S. Berrah, H. Abid, and M. A. Saeed, "Structural, electronic and optical properties for chalcopyrite semiconducting materials: *ab-initio* computational study," *Optik*, vol. 169, pp. 69–76, Sep. 2018, https://doi.org/10.1016/j.ijleo.2018.05.044.

[36] M. I. Alonso, K. Wakita, J. Pascual, M. Garriga, and N. Yamamoto, "Optical functions and electronic structure of $CuInSe_2$, $CuGaSe_2$, $CuInS_2$, and $CuGaS_2$," *Physical Review B*, vol. 63, no. 7, Jan. 2001, Art. no. 075203, https://doi.org/10.1103/PhysRevB.63.075203.

[37] S. Adachi, *Properties of Semiconductor Alloys: Group-IV, III-V and II-VI Semiconductors*. London, UK: John Wiley & Sons, 2009.

[38] C. F. Klingshirn, *Semiconductor Optics*. Berlin, Heidelberg: Springer, 2012.

[39] M. Gajdoš, K. Hummer, G. Kresse, J. Furthmüller, and F. Bechstedt, "Linear optical properties in the projector-augmented wave methodology," *Physical Review B*, vol. 73, no. 4, Jan. 2006, Art. no. 045112, https://doi.org/10.1103/PhysRevB.73.045112.

[40] A. Soni *et al.*, "Electronic and Optical Modeling of Solar Cell Compounds CuGaSe2 and CuInSe2," *Journal of Electronic Materials*, vol. 40, no. 11, pp. 2197–2208, Nov. 2011, https://doi.org/10.1007/s11664-011-1739-1.

[41] S. Levcenko *et al.*, "Optical spectra and energy band structure of single crystalline CuGaS2 and CuInS2," *Journal of Physics: Condensed Matter*, vol. 19, no. 45, Oct. 2007, Art. no. 456222, https://doi.org/10.1088/0953-8984/19/45/456222.

[42] J. C. Rife, R. N. Dexter, P. M. Bridenbaugh, and B. W. Veal, "Optical properties of the chalcopyrite semiconductors $ZnGeP_2$, $ZnGeAs_2$, $CuGaS_2$, $CuAlS_2$, $CuInSe_2$, and $AgInSe_2$," *Physical Review B*, vol. 16, no. 10, pp. 4491–4500, Nov. 1977, https://doi.org/10.1103/PhysRevB.16.4491.

[43] M. Othman, E. Kasap, and N. Korozlu, "The structural, electronic and optical properties of $In_xGa_{1-x}P$ alloys," *Physica B: Condensed Matter*, vol. 405, no. 10, pp. 2357–2361, May 2010, https://doi.org/10.1016/j.physb.2010.02.051.

[44] A. Mouhoub, F. Khaled, and A. Bouloufa, "Performance Analysis of Ultrathin Cu(In,Ga)Se2 Solar Cells with Backwall Superstrate Configuration Using AMPS-1D," *Engineering, Technology & Applied Science Research*, vol. 12, no. 6, pp. 9687–9691, Dec. 2022, https://doi.org/10.48084/etasr.5341.

[45] N. Bouarissa and H. Aourag, "Effective masses of electrons and heavy holes in InAs, InSb, GaSb, GaAs and some of their ternary compounds," *Infrared Physics & Technology*, vol. 40, no. 4, pp. 343–349, Aug. 1999, https://doi.org/10.1016/S1350-4495(99)00020-1.